An all-in-one integrating strategy for designing platinum(II)-based supramolecular polymers for photocatalytic hydrogen evolution

Yanyan Qin, Pengfei She, Yidi Wang, and Wai-Yeung Wong**

Y. Y. Qin, P. F. She, Y. D. Wang, W.-W. Wong

Department of Applied Biology and Chemical Technology and Research Institute for Smart Energy. The Hong Kong Polytechnic University, Hung Hom, Hong Kong P. R. China and The Hong Kong Polytechnic University Shenzhen Research. Institute, Shenzhen 518057, P. R. China.

E-mail: pengfei.she@polyu.edu.hk, wai-yeung.wong@polyu.edu.hk

Keywords: Chalcogenoviologen, Platinum(II)-based supramolecular polymers, Integrated functional system, Charge transfer, Photocatalytic hydrogen evolution

Organic polymer photocatalysts have achieved significant progress in photocatalytic hydrogen evolution, while developing the integrated organic polymers possessing the functions of photosensitizer, electron transfer mediator, and catalyst simultaneously is urgently needed and presents a great challenge. Considering that chalcogenoviologens are able to act as photosensitizers and electron-transfer mediators, we designed a series of chalcogenoviologen-containing platinum(II)-based supramolecular polymers, which exhibited strong visible light-absorbing ability and suitable bandgap for highly efficient photocatalytic hydrogen evolution without the use of a cocatalyst. Among these "all-in-one" polymers, 9a exhibited the best photocatalytic performance with a hydrogen evolution rate (HER) of 3.09 mmol g^{-1} h^{-1} under visible light (>420 nm) irradiation. Experimental and theoretical calculations reveal that the distinct intramolecular charge transfer characteristics and heteroatom N in terpyridine units play an important role in photocatalysis. This work could provide new insights into the design of metallo-supramolecular polymers with finely tuned components for photocatalytic hydrogen evolution from water.

1. Introduction

Given the escalating global energy demand, hydrogen energy derived from solar-driven water splitting is considered as a renewable and eco-friendly alternative to fossil fuels.[1–3] Photocatalytic hydrogen evolution has become a promising and sustainable strategy in solar

energy utilization. Substantial efforts have been devoted to the development of efficient photocatalytic systems. In particular, organic polymer photocatalysts have attracted considerable attention due to their diverse structures, flexible synthetic methods, and tunable optical bandgaps and carrier transport properties.[4,5] At present, organic polymer photocatalysts, such as graphitic carbon nitride (g-C_3N_4),[6–8] linear conjugated polymers,[9–11] polymer dots,[12–14] and porous materials like conjugated microporous polymers (CMPs),[15–17] metal-organic frameworks (MOFs),[18–20] covalent organic frameworks (COFs)[21–23] and covalent triazine frameworks (CTFs),[24–26] have been extensively exploited and studied. However, the photocatalytic performance is often restricted by the limited visible light absorption and weak charge separation/transfer. Moreover, the low dielectric properties of polymers often lead to strong excitonic effects,[27–29] which are detrimental to photocatalysis. To date, various strategies have been developed to improve photogenerated charge carrier separation and transport, such as surface modification,[30–32] chemical doping,[33–35] cocatalyst deposition[36–38] and construction of donor-acceptor (D-A) junctions.[39–41] Besides, electron transfer mediator (ETM) engineering also provides a good choice.[42,43]

As we know, viologen (MV^{2+}), as an ideal ETM, can accept one electron to form the corresponding cationic radical ($MV^{+\bullet}$) *via* photoinduced electron transfer (PET) process, which plays a vital role in photocatalytic reaction.[44–46] Compared with conventional viologens, chalcogenoviologens, a kind of viologen derivatives, exhibit more redox centers and narrower band gaps due to the effective σ*–π* hyperconjugation. As a consequence, chalcogenoviologens are able to act as photosensitizers (PS) and ETMs, promoting the rapid electron transfer in photocatalytic system.[47–50] However, the intermolecular PET from PS to ETM to catalyst will greatly reduce the utilization of electrons and hinder the efficiency of H_2 generation due to long intermolecular electron transfer distance. Therefore, incorporating the PS, ETM and catalyst into a unified photocatalytic system might minimize the electron transfer distance between PS and active sites, reducing the possibility of electron–hole recombination and enhancing the photocatalytic performance.[51–54]

In photocatalysis, suitable optical gap always contributes to the exciton-generation. Meanwhile, introducing a metal into the skeleton of polymers could greatly enhance the light-harvesting *via* a metal-to-ligand charge transfer (MLCT) process,[55] which is highly desired in photocatalysis. Besides, the utilization of D-A junctions could also provide an efficient intramolecular charge transfer (ICT) in organic polymers,[39] which is conducive to photocatalysis. Taking the above considerations into account, we have rationally designed and synthesized a series of chalcogenoviologen-containing platinum(II)-based supramolecular

polymers (PtSPs) with donor (D)-acceptor (A) structure (**Figure 1**), which possess the advantages of organic polymers and viologen-based derivatives, and their photocatalytic activities for hydrogen production from water are investigated carefully. By introducing different types of donors, the PtSPs exhibited the tunable optical, physical, and photocatalytic properties. Our designed organometallic polymers not only integrate the functions of PS, ETM and catalyst, but also afford a highly efficient electron transfer process. Thus, the designed polymer **9a** displays an excellent hydrogen evolution rate (HER) of 3.09 mmol g^{-1} h^{-1} under visible light (>420 nm) irradiation without the need of a cocatalyst. To our best knowledge, this efficiency is the highest value for viologen-based organic photocatalytic systems, demonstrating an efficient material design for photocatalysis. In addition, the influence of the linkers on the photocatalytic performance for the resulting polymers is compared and discussed.

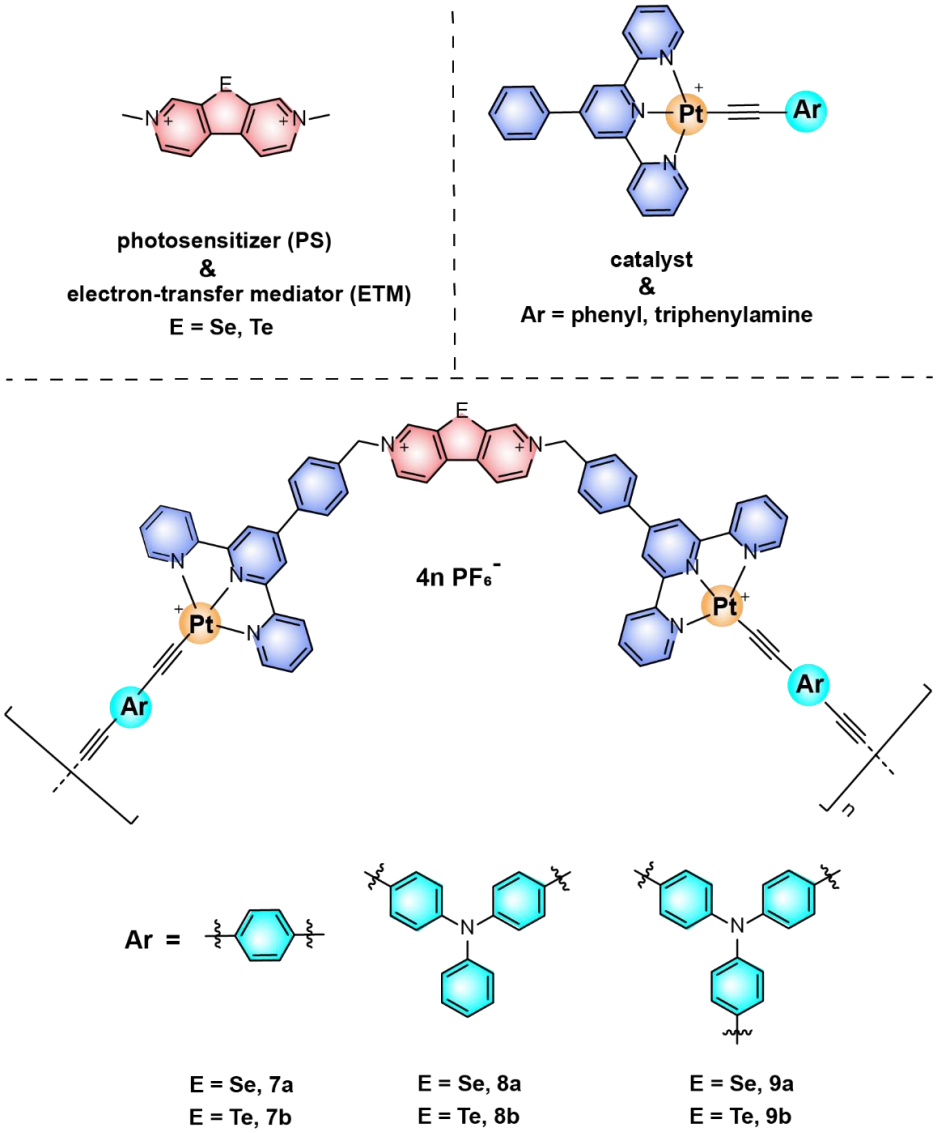

Figure 1. The chemical structures of chalcogenoviologen-containing platinum(II)-based supramolecular polymers.

2. Results and Discussion

2.1. Characterization of PtSPs

As shown in **Figure 2**a and Figure S1a, the observed broad peaks from 160 to 110 ppm in the solid-state ^{13}C NMR spectra of polymers are derived from the aromatic carbon atoms, and the small peaks located at *ca.* 105 ppm are assigned to C≡C, confirming the successful polymerization. Compared with **7a**, the peaks of C≡C in **8a** and **9a** are dramatically up-field shifted owing to the existence of strong electron-donating triphenylamine unit. Unlike the FT-IR spectra of their precursors, the disappearance of the peaks at *ca.* 3300 cm^{-1} (≡C-H) at lower frequency and the appearance of the new characteristic signals of C≡C at *ca.* 2100 cm^{-1} demonstrate the formation of polymer (Figure 2b, Figure S2). Meanwhile, the surface compositions and valence states of all polymers are also characterized by XPS (Figure 2c, Figure S3). Their XPS survey spectra give good evidence for the existence of C, N, Se, Pt, P and F elements. The C 1s spectra of polymer can be deconvoluted into four peaks, which are assigned to the C-Pt, C-C/C=C (sp^2-C of the aromatic rings), C-N/C=N (carbon atoms from the pyridine unit) and C-Se, respectively, indicating the successful introduction of C≡C group into the frameworks. For the N 1s spectra, polymers exhibit four distinct lines that correspond to the N-Pt, N-C, N=C and $C–N^+$, respectively. The Pt 4f XPS spectra show two main peaks and two satellite peaks (due to the shake-down mechanism), corresponding to Pt $4f_{7/2}$ and Pt $4f_{5/2}$, respectively, which are characteristic of Pt^{2+} species. The detailed bonding energies for polymer **7a**, **8a** and **9a** are shown in Table S1. Elemental analysis also supports the structures of polymers as proposed (Table S2). TGA analysis clarifies the good thermal stabilities for all polymers (Figure S4). PXRD patterns of all polymers present broad and low intensity peaks ranging from 15° to 35° (2θ), suggesting that these polymers are disordered and amorphous (Figure 2d, Figure S1b).

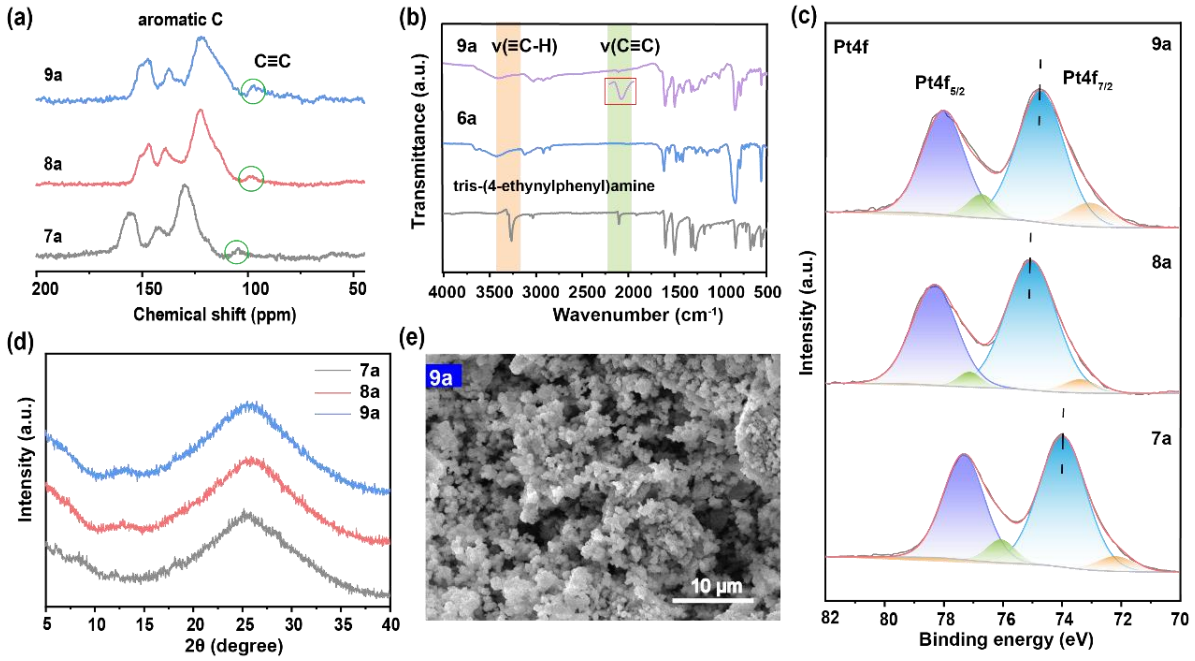

Figure 2. (a) Solid-state ^{13}C NMR spectra of polymers **7a**, **8a** and **9a**; (b) FT-IR spectra of monomers and polymer **9a**; (c) the Pt 4f XPS spectra of polymers **7a**, **8a** and **9a**; (d) the PXRD patterns of polymers **7a**, **8a** and **9a**; (e) SEM image of polymer **9a**.

2.2. Morphological study

The morphologies of the solid state of PtSPs were further explored by scanning electron microscopy (SEM). As displayed in Figure 2e and Figure S5, their SEM images show a fused particle-like shape. The porosities of all polymers were further examined *via* an adsorption experiment at 77 K. The isotherms and pore size distribution curves obtained using the Brunauer−Emmett−Teller (BET) and Barrett−Joyner−Halenda (BJH) methods are summarized in Figures S6 and S7. Polymer **9a** exhibits higher BET surface areas of 33.26 $m^2\ g^{-1}$, and the pore volume of 0.12 $cm^3\ g^{-1}$ at P/P_0 = 0.99, respectively. By contrast, the linear polymers **7a** and **8a** show slightly lower BET surface areas of 21.73 and 28.09 $m^2\ g^{-1}$, which could be attributed to the strong structure stacking induced by π–π interactions.[56, 57] The high BET surface area and large pore volume of **9a** provide more active sites for photocatalytic H_2 evolution and accessible channels for electron transport.

Table 1. Photophysical properties and photocatalytic performances of all polymers.

		experimental			calculated		
polymer	HER [μmol h^{-1} g^{-1}] [a]	HOMO /eV [e]	LUMO /eV [d]	E_g/eV [c]	HOMO /eV [f]	LUMO /eV [f]	E_g/eV [f]
7a	0.22/0.37 [b]	-5.24	-3.54	1.70	-5.57	-3.97	1.60
7b	0.11	-5.27	-3.51	1.76	-5.57	-3.91	1.66
8a	0.37/0.64[b]	-5.10	-3.56	1.54	-5.05	-3.97	1.08
8b	0.16	-5.11	-3.52	1.59	-5.05	-3.92	1.13
9a	1.76/3.09[b]	-5.07	-3.59	1.48	-5.04	-3.99	1.05
9b	0.56	-5.06	-3.61	1.45	-5.05	-3.94	1.01

[a] Reaction conditions: polymer (1 mg), MeOH/H_2O/TEA (1/1/0.1 in vol, 4 mL), 300 W Xe lamp with cut-off filter > 420 nm; [b] reaction conditions: polymer (1 mg), MeOH/H_2O/TEA (5/1/0.1 in vol, 4 mL); [c] calculated from Tauc plots; [d] LUMO derived by CV; [e] HOMO derived by subtracting E_g from E_{HOMO}, i.e., $E_{HOMO} - E_g$; [f] determined from the DFT calculations.

2.3. Optical properties and energy diagram

The optoelectronic properties of polymers can be effectively tailored through molecular engineering. As shown in **Figure 3**a and Figure S8, the ultraviolet-visible (UV-Vis) diffuse reflectance spectra of all polymers exhibit strong absorption in the visible region with an absorption edge reaching about 1000 nm, which are significantly red-shifted relative to the monomer Pt complex owing to the extended degree of π-conjugation. The introduction of triphenylamine slightly lowered the energy levels due to its better electron-donating ability as compared with the phenyl unit, leading to the production of narrower bandgap polymers.[58] According to the Tauc plots, the optical band gaps (E_g) of polymers **7**-**9** range from 1.45 to 1.76 eV (Figure 3b, Table 1), suggesting that the E_g values can be modulated by varying the structures of the donor comonomers and heavy atoms. To determine the energy band, cyclic voltammetry (CV) measurement was conducted by using ferrocene/ferrocenium (Fc/Fc^+) reference as an internal standard (Figure S9). As shown in Figure 3c, the LUMO levels of polymers range from -3.51 to -3.61 eV, which are higher than the water reduction potential, suggesting that the thermodynamic force can drive the half reaction for water-splitting.[59]

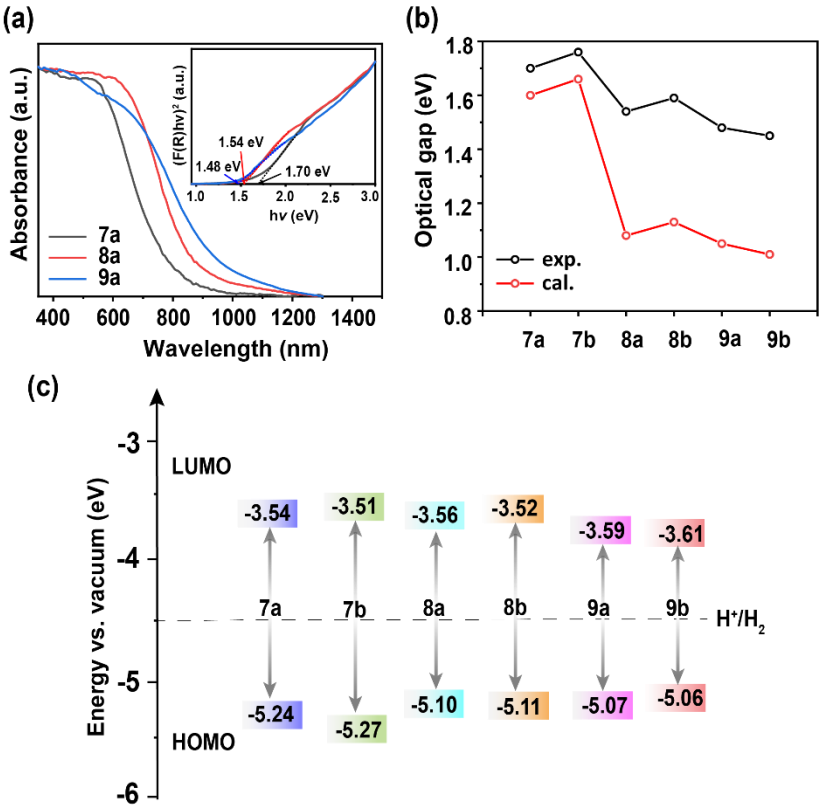

Figure 3. (a) UV-Vis diffuse reflectance spectra of polymers **7a**, **8a** and **9a**, inset: Tauc plots of the corresponding polymers; (b) experimental and calculated energy bandgaps of all polymers; (c) the energy band diagram, where the gray dotted line represents the redox potential of H^+/H_2.

Additionally, according to the Mott-Schottky plots (Figure S10), the positive slopes of Mott-Schottky curves indicate these polymers are n-type organic semiconductors.[60] The flat-band potentials are estimated to be –1.18, –1.21, –1.20, –1.22, –1.12 and − 1.13 V vs. Ag/AgCl electrode for **7a**, **7b**, **8a**, **8b**, **9a** and **9b**, respectively. The conduction band (CB) potential is roughly equal to the flat-band potential for an n-type semiconductor.[61, 62] According to the bandgap and the CB position of the polymers, the valence band (VB) of polymers are calculated to be ca. –0.98, –1.01, –1.00, –1.02, –0.92 and – 0.93 V vs. normalized hydrogen electrode (NHE), respectively. These data are moderately consistent with the results from CV measurements.

To evaluate the disparity in E_g and the absorption ability of these polymers, density functional theory (DFT) calculations of the fragmental structures of polymers were performed (Figure S11). The highest occupied molecular orbitals (HOMOs) of polymers are mainly distributed over the ethynyl linkers of polymers and to a smaller extent on the metal Pt, while the lowest unoccupied molecular orbitals (LUMOs) are mainly localized on the chalcogenoviologen

groups. It is observed that the HOMOs and LUMOs are fully separated, leading to a decline in the recombination of electron–hole pairs. This kind of distinct intramolecular charge transfer (ICT) from donor to acceptor will improve charge separation. Additionally, the calculated E_g values (Figure 3b) of the polymers follow the order of **9a** < **8a** < **7a**, which matches well with the experimentally measured results. Furthermore, based on the Mulliken atomic charges calculations, the red color indicates electron-withdrawing ability. An increased charge value signifies a stronger electron-withdrawing ability of N atom in the polymer structure. It is evident that the N atom in terpyridine has the lowest value of Mulliken atomic charges (Figure S12), revealing the highest concentration of electron on N atoms. Thus, as the terpyridine content in polymer increases, polymer **9a** shows an exceptional electron-capture ability of N atoms.

2.4. Photocatalytic hydrogen evolution

To establish the photocatalytic system, a sacrificial agent (SA) was added to a cosolvent of MeOH and H_2O, with 1 mg polymer dispersed in the solution. Methanol was added to facilitate the mixing of the otherwise immiscible SA/water system, as well as to improve the dispersion of the photocatalysts in water. Different types of SAs would exhibit different influences on the photocatalytic system.[63-65] For the initial photocatalysis test, three widely used SAs, triethylamine (TEA), triethanolamine (TEOA), and ascorbic acid (AA) were selected, and no additional metal cocatalyst (e.g. Pt) was added. As displayed in Figure S13, the photocatalytic activity of polymer **7a** is much higher in TEA solutions than in AA or TEOA solutions. Therefore, TEA is chosen as the SA in subsequent optimization tests. After testing six samples in MeOH/H_2O/TEA (1:1:0.1, v/v/v) system, the best performance for photocatalytic H_2 evolution (**Figure 4**a) occurs when polymer **9a** as photocatalyst is used. The HERs for all prepared polymers are 0.22 (for **7a**), 0.11 (for **7b**), 0.37 (for **8a**), 0.16 (for **8b**), 1.76 (for **9a**) and 0.56 mmol g^{-1} h^{-1} (for **9b**), respectively. The HERs of the Se-containing polymers are significantly higher than those of the Te-containing polymers, presumably because of their stronger light absorption and weak heavy atom effect, thereby favoring photocatalytic activity.

It has been reported that high hydrophilicity combined with a narrow water contact angle can increase the interaction between the photocatalytic reaction solution and the polymer surface, resulting in greater photocatalytic activity.[36] So, the water contact angle measurements were carried out to compare polymer hydrophilicity (Figure S14). The Se-containing polymers show better hydrophilicity than the Te-containing polymers due to their smaller contact angles. To better understand the structure–property relationships of our designed polymers, we mainly discuss Se-containing polymers here. The contact angles of polymers **7a**, **8a** and **9a** are 55.72°,

51.69°, and 45.55°, respectively. The higher hydrophilicity of polymer **9a** can be attributed to the higher terpyridine content and additional heteroatoms, particularly the N atom.[26] The increased number of hydrophilic heteroatoms functions as active sites for electron accumulation in the process of H_2 production. Thus, the polymer **9a** provides the highest HER. Overall, we conclude that introducing the strong donor and increasing the nitrogen content in the backbones of chalcogenoviologen-containing PtSPs result in enhanced H_2 production from water.

In addition, the photocatalytic hydrogen production activity could be enhanced through optimization of the cosolvent ratio. As shown in Figure S15a-c, the photocatalytic activities of polymers **7a**, **8a** and **9a** are remarkably increased as the content of MeOH is increased. The HERs of polymers **7a**, **8a** and **9a** are up to 0.37, 0.64 and 3.09 mmol g^{-1} h^{-1} in MeOH/H_2O/TEA (5:1:0.1, v/v/v) system, respectively. These values are significantly higher than that reported in viologen-containing photocatalytic hydrogen production system.[48, 50, 52] Given the highest HER value of **9a**, we further explored the effect of concentration of SA on the HER performance. The best photocatalytic hydrogen production performance occurs when 0.1% vol TEA is used (Figure S15d). The apparent quantum yields (AQYs) of **9a** are measured to be 0.42%, 0.43%, 0.25%, 0.12% and 0.06% at 420, 450, 500, 550 and 600 nm, respectively (Figure 4b). Table S4 summarizes the HERs of some viologen-based photocatalysts under visible-light irradiation; our polymers, after adjusting the photocatalytic settings, afford comparable HERs and excellent AQY at 450 nm irradiation. Under the optimized conditions, long-term photocatalytic cycling experiments were carried out. Polymer **9a** has good photostability and durability, as evidenced by the continuous irradiation for ~12 h (Figure 4c). The stability of the photocatalyst before and after illumination was confirmed by examining the XRD patterns, FT-IR, and UV spectra (Figure S16).

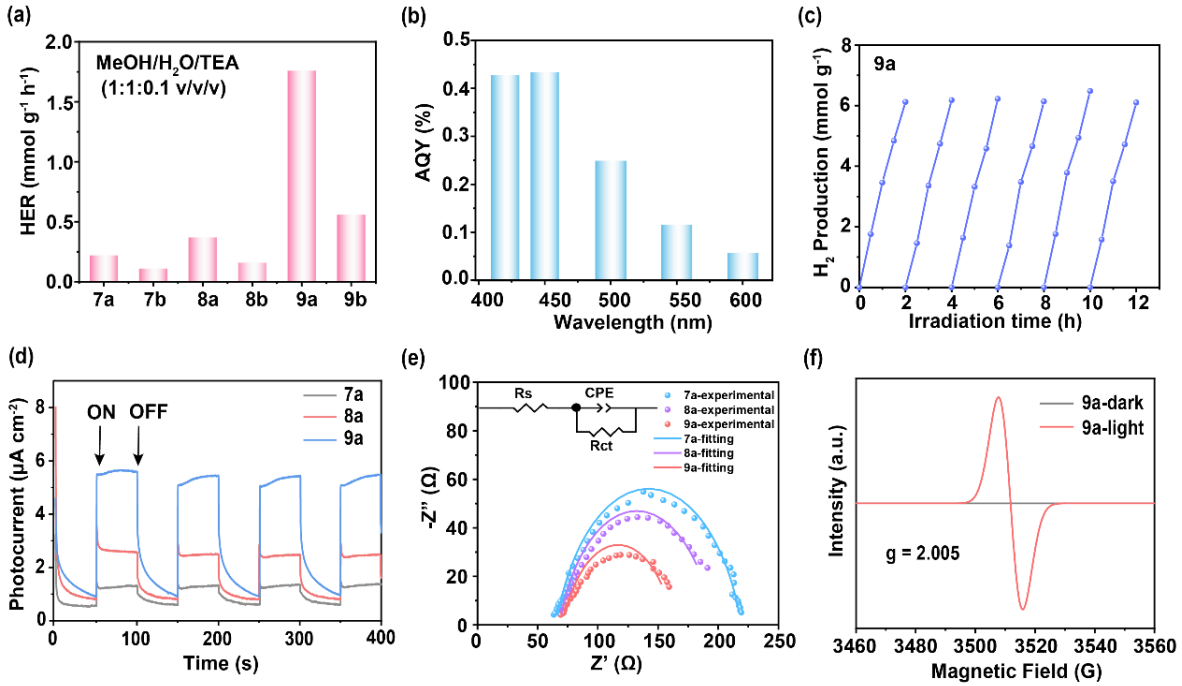

Figure 4. (a) Photocatalytic H_2 evolution rates of all polymers; (b) the AQYs of polymer **9a** under different wavelengths of light; (c) long-term H_2 production of polymer **9a**; (d) photocurrent response spectra; (e) the electrochemical impedance spectra; (f) EPR spectra of **9a** under light irradiation and dark. Note: Rs is the solution internal resistance; Rct is the solution charge transfer resistance; CPE is the constant phase angle element.

2.5. Mechanism study

Considering the significant difference in structure and properties between linear and porous polymers, the charge separation and transfer properties of all polymers were further studied by a combined test of photocurrent and electrochemical impedance spectroscopy (Figures 4d-e, and Figure S17). For Se-containing polymers, **9a** shows higher photocurrent response than **8a** and **7a** under light illumination (Figure 4d). Moreover, **9a** displays the smallest arc radius in the Nyquist plot (Figure 4e, Table S3), suggesting that the interface of **9a** exhibits the best charge migration ability. Overall, the photocatalytic activity of polymers is in the order of **9a** > **8a** > **7a**, which is in good agreement with the charge separation efficiency as mentioned above. The excellent optoelectronic properties of **9a** should be ascribed to its broader absorption range, faster charge transfer, and lower probability of excitons recombination. Furthermore, the charge separation efficiency of **9a** was also evaluated by electron paramagnetic resonance (EPR) spectroscopy. Under irradiation, **9a** shows a higher EPR signal at g = 2.005 compared to that under darkness, indicating the presence of the photo-generated electron-hole pairs (Figure 4f).

On the basis of the aforementioned experimental and theoretical results, a probable mechanism for photocatalytic H_2 evolution is proposed (**Figure 5**). After being excited under light, the distinctive intramolecular charge transfer (ICT) in the D-A type polymers triggers a rapid electron transfer from the donor to the acceptor. Chalcogenoviologen, as the ETM, accelerates the electron transfer from the PS to the active site, reducing the possibility of electron–hole recombination and enhancing the photocatalytic performance. Compared with the linear polymers, the porous polymers could form electron delivery channels and offer more active sites. Moreover, the narrowed band gap enables porous polymers to efficiently utilize visible light to activate more photoinduced charge carriers than that of the linear polymers. Finally, the porous structure can markedly improve the photocatalytic H_2 evolution.

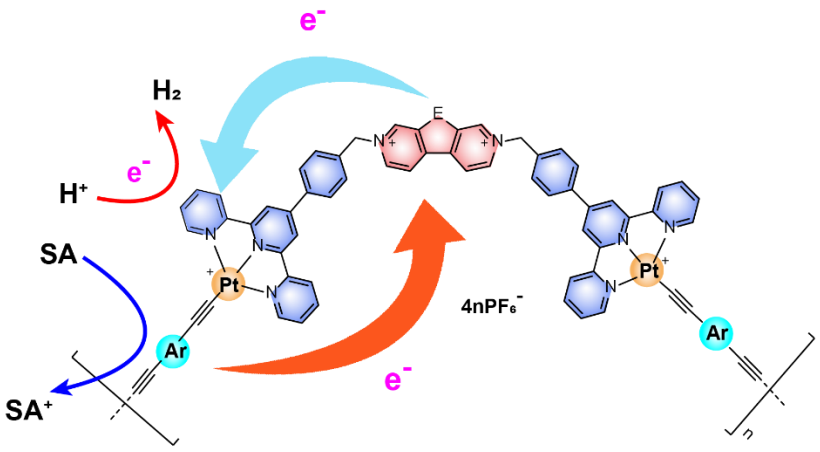

Figure 5. Proposed mechanism for the photocatalytic hydrogen production.

3. Conclusion

In summary, we have designed and synthesized a series of chalcogenoviologen-containing PtSPs for efficient hydrogen evolution, with PS, ETM and photocatalyst all integrated in one system. The three-module functional polymers can greatly optimize the light absorption ability and exciton-separation efficiency. Among them, polymer **9a** demonstrates excellent photocatalytic efficiency with an HER of 3.09 mmol g^{-1} h^{-1} under visible light (>420 nm) irradiation and an AQY of 0.43% at 450 nm with TEA as SA and without any additional cocatalyst. DFT calculations suggest that the distinct ICT characteristics and heteroatom N in terpyridine units play an important role in photocatalysis. Meanwhile, the efficient ICT inhibits the recombination of the carriers in the polymer caused by the strong excitonic effect, thus improving the photocatalytic performance. These results also demonstrate the successful all-in-

one construction strategy in D-A type PtSPs, providing new insights into the design and synthesis of multifunctional polymers with prominent photocatalytic performance.

4. Experimental section

4.1. Materials

Lithium diisopropylamide (LDA, 2 M in THF), anhydrous copper (II) chloride, 3-bromopyridine, ammonium hydroxide (28%–30%), *n*-butyllithium solution (2.5 M in hexanes), selenium powder, sodium sulfide nonahydrate, 4-methylbenzaldehyde, 2-acetylpyridine, N-bromosuccinimide, ammonium hexafluorophosphate, 4,4′-dibromotriphenylamine, tris(4-bromophenyl)amine, dipotassium tetrachloroplatinate (K_2PtCl_4, 99%), tetrakis(triphenylphosphine)palladium(0), copper(I) iodide, triethylamine, trimethylsilylacetilene, potassium carbonate, anhydrous N,N-dimethylformamide (DMF) and anhydrous tetrahydrofuran (THF) were purchased from Energy Chemical. Deionized water was applied throughout the whole synthesis experiment. All used other reagents were of analytical grade and used without additional purification.

4.2. Synthesis of platinum(II)-based supramolecular polymers (PtSPs)

The PtSPs were synthesized by copolymerization *via* a Sonogashira reaction between chalcogenoviologen-containing platinum(II) chloride complexes and alkynyl compounds, in which different kinds of organic linkers were chosen to investigate their structure-property relationship. In a typical reaction, a flask was charged with the two monomers, copper(I) iodide, triethylamine and dry DMF, then the mixture was degassed and filled with nitrogen for three times, then the mixture was stirred at 100 °C for 48 h. After cooling to room temperature, the precipitate was isolated *via* vacuum filtration and washed with dichloromethane, DMF and MeOH, respectively. Then the solid was washed using Soxhlet with MeOH and acetone for 12 hours. After drying the materials under high vacuum, the polymers were obtained. The detailed synthetic procedures for the monomers and polymers are described in the Supporting Information.

4.3. Polymer characterizations

Because the polymers are cross-linked materials and insoluble in organic solvents, their chemical structures cannot be characterized by most traditional instrumentations. Therefore, they were subsequently characterized by solid-state ^{13}C NMR spectroscopy, Fourier transform

infrared (FT-IR) spectroscopy, powder X-ray diffraction (PXRD), X-ray photoelectron spectroscopy (XPS), scanning electron microscopy (SEM) and elemental analysis.

4.4. Photocatalytic test

Photocatalytic hydrogen evolution experiments of the polymers were conducted at ambient temperature using visible light irradiation. The photocatalytic system containing a mixture of **PtSPs** (1 mg), a sacrificial agent (SA) (10 vol.%), MeOH and H_2O was sealed in a 20 mL Pyrex bottle. Before irradiation under a 300 W Xe-lamp (CEL-HXF300, CEAULIGHT, Beijing) with a cut-off filter > 420 nm, the mixture was bubbled with Ar for 30 min to remove air thoroughly, and 300 μL CH_4 was injected into the bottle. The generated gases were analyzed by gas chromatography (Shimadzu, GC2030) and calculated according to the normalized curve.

Supporting Information

Supporting Information is available from the Wiley Online Library or from the author.

Acknowledgements

This work was supported by the RGC Senior Research Fellowship Scheme (SRFS2021-5S01); the Hong Kong Research Grants Council (PolyU 15307321); Research Institute for Smart Energy (CDAQ) and Miss Clarea Au for the Endowed Professorship in Energy (847S); National Natural Science Foundation of China (52073242 and 62205277).

Conflict of interest

There are no conflicts to declare.

Received: ((will be filled in by the editorial staff))

Revised: ((will be filled in by the editorial staff))

Published online: ((will be filled in by the editorial staff))

References

[1] X. Tao, Y. Zhao, S. Wang, C. Li, R. Li, *Chem. Soc. Rev.* **2022**, *51*, 3561.

[2] H. Song, S. Luo, H. Huang, B. Deng, J. Ye, *ACS Energy Lett.* **2022**, *7*, 1043.

[3] Y. Wang, A. Vogel, M. Sachs, R. S. Sprick, L. Wilbraham, S. J. A. Moniz, R. Godin, M. A. Zwijnenburg, J. R. Durrant, A. I. Cooper, J. Tang, *Nat. Energy* **2019**, *4*, 746.

[4] T. Banerjee, F. Podjaski, J. Kröger, B. P. Biswal, B. V. Lotsch, *Nat. Rev. Mater.* **2021**, *6*, 168.

[5] C. Zhao, Z. Chen, R. Shi, X. Yang, T. Zhang, *Adv. Mater.* **2020**, *32*, 1907296.

[6] J. Liang, X. Yang, Y. Wang, P. He, H. Fu, Y. Zhao, Q. Zou, X. An, *J. Mater. Chem. A* **2021**, *9*, 12898.

[7] C. Liu, Y. Zhang, F. Dong, A. H. Reshak, L. Ye, N. Pinna, C. Zeng, T. Zhang, H. Huang, *Appl. Catal. B: Environ.* **2017**, *203*, 465.

[8] L. Lin, Z. Yu, X. Wang, *Angew. Chem. Int. Ed.* **2019**, *58*, 6164.

[9] P. Xie, C. Han, S. Xiang, S. Jin, M. Ge, C. Zhang, J.-X. Jiang, *Chem. Eng. J.* **2023**, *459*, 141553.

[10] Z.-R. Tan, Y.-Q. Xing, J.-Z. Cheng, G. Zhang, Z.-Q. Shen, Y.-J. Zhang, G. Liao, L. Chen, S.-Y. Liu, *Chem. Sci.* **2022**, *13*, 1725.

[11] W.-C. Lin, J. Jayakumar, C.-L. Chang, L.-Y. Ting, M. H. Elsayed, M. Abdellah, K. Zheng, A. M. Elewa, Y.-T. Lin, J.-J. Liu, W.-S. Wang, C.-Y. Lu, H.-H. Chou, *Appl. Catal. B: Environ.* **2021**, *298*, 120577.

[12] C.-L. Chang, W.-C. Lin, C.-Y. Jia, L.-Y. Ting, J. Jayakumar, M. H. Elsayed, Y.-Q. Yang, Y.-H. Chan, W.-S. Wang, C.-Y. Lu, P.-Y. Chen, H.-H. Chou, *Appl. Catal. B: Environ.* **2020**, *268*, 118436.

[13] M. H. Elsayed, J. Jayakumar, M. Abdellah, T. H. Mansoure, K. Zheng, A. M. Elewa, C.-L. Chang, L.-Y. Ting, W.-C. Lin, H.-h. Yu, W.-H. Wang, C.-C. Chung, H.-H. Chou, *Appl. Catal. B: Environ.* **2021**, *283*, 119659.

[14] P.-J. Tseng, C.-L. Chang, Y.-H. Chan, L.-Y. Ting, P.-Y. Chen, C.-H. Liao, M.-L. Tsai, H.-H. Chou, *ACS Catal.* **2018**, *8*, 7766.

[15] A. M. Elewa, M. H. Elsayed, A. F. M. El-Mahdy, C.-L. Chang, L.-Y. Ting, W.-C. Lin, C.-Y. Lu, H.-H. Chou, *Appl. Catal. B: Environ.* **2021**, *285*, 119802.

[16] Z.-A. Lan, W. Ren, X. Chen, Y. Zhang, X. Wang, *Appl. Catal. B: Environ.* **2019**, *245*, 596.

[17] A. F. Saber, A. M. Elewa, H.-H. Chou, A. F. M. El-Mahdy, *Appl. Catal. B: Environ.* **2022**, *316*, 121624.

[18] W. Wang, X. Xu, W. Zhou, Z. Shao, *Adv. Sci.* **2017**, *4*, 1600371.

[19] X. Chen, S. Xiao, H. Wang, W. Wang, Y. Cai, G. Li, M. Qiao, J. Zhu, H. Li, D. Zhang, Y. Lu, *Angew. Chem. Int. Ed.* **2020**, *59*, 17182.

[20] X. Feng, Y. Pi, Y. Song, C. Brzezinski, Z. Xu, Z. Li, W. Lin, *J. Am. Chem. Soc.* **2020**, *142*, 690.

[21] D.-G. Wang, T. Qiu, W. Guo, Z. Liang, H. Tabassum, D. Xia, R. Zou, *Energy Environ. Sci.* **2021**, *14*, 688.

[22] C. Li, J. Liu, H. Li, K. Wu, J. Wang, Q. Yang, *Nat. Commun.* **2022**, *13*, 2357.

[23] I. Ahmed, S. H. Jhung, *Coord. Chem. Rev.* **2021**, *441*, 213989.

[24] Y. Yang, H. Niu, L. Xu, H. Zhang, Y. Cai, *Appl. Catal. B: Environ.* **2020**, *269*, 118799.

[25] L. Guo, Y. Niu, H. Xu, Q. Li, S. Razzaque, Q. Huang, S. Jin, B. Tan, *J. Mater. Chem. A* **2018**, *6*, 19775.

[26] Z. Qian, Z. J. Wang, K. A. I. Zhang, *Chem. Mater.* **2021**, *33*, 1909.

[27] H. Wang, S. Jin, X. Zhang, Y. Xie, *Angew. Chem. Int. Ed.* **2020**, *59*, 22828.

[28] Y. Qian, D. Li, Y. Han, H.-L. Jiang, *J. Am. Chem. Soc.* **2020**, *142*, 20763.

[29] Z.-A. Lan, G. Zhang, X. Chen, Y. Zhang, K. A. I. Zhang, X. Wang, *Angew. Chem. Int. Ed.* **2019**, *58*, 10236.

[30] W. Chen, L. Wang, D. Mo, F. He, Z. Wen, X. Wu, H. Xu, L. Chen, *Angew. Chem. Int. Ed.* **2020**, *59*, 16902.

[31] Y. Xiang, X. Wang, L. Rao, P. Wang, D. Huang, X. Ding, X. Zhang, S. Wang, H. Chen, Y. Zhu, *ACS Energy Lett.* **2018**, *3*, 2544.

[32] F. Li, D. Wang, Q.-J. Xing, G. Zhou, S.-S. Liu, Y. Li, L.-L. Zheng, P. Ye, J.-P. Zou, *Appl. Catal. B: Environ.* **2019**, *243*, 621.

[33] G. Shu, Y. Li, Z. Wang, J.-X. Jiang, F. Wang, *Appl. Catal. B: Environ.* **2020**, *261*, 118230.

[34] S. Li, M.-F. Wu, T. Guo, L.-L. Zheng, D. Wang, Y. Mu, Q.-J. Xing, J.-P. Zou, *Appl. Catal. B: Environ.* **2020**, *272*, 118989.

[35] Y. Zhu, X. Chen, Y. Cao, W. Peng, Y. Li, G. Zhang, F. Zhang, X. Fan, *Chem. Commun.* **2019**, *55*, 1434.

[36] C. Shu, C. Han, X. Yang, C. Zhang, Y. Chen, S. Ren, F. Wang, F. Huang, J.-X. Jiang, *Adv. Mater.* **2021**, *33*, 2008498.

[37] R.-B. Wei, Z.-L. Huang, G.-H. Gu, Z. Wang, L. Zeng, Y. Chen, Z.-Q. Liu, *Appl. Catal. B: Environ.* **2018**, *231*, 101.

[38] H. Dong, X.-B. Meng, X. Zhang, H.-L. Tang, J.-W. Liu, J.-H. Wang, J.-Z. Wei, F.-M. Zhang, L.-L. Bai, X.-J. Sun, *Chem. Eng. J.* **2020**, *379*, 122342.

[39] Z.-A. Lan, M. Wu, Z. Fang, X. Chi, X. Chen, Y. Zhang, X. Wang, *Angew. Chem. Int. Ed.* **2021**, *60*, 16355.

[40] J. Kosco, M. Bidwell, H. Cha, T. Martin, C. T. Howells, M. Sachs, D. H. Anjum, S. Gonzalez Lopez, L. Zou, A. Wadsworth, W. Zhang, L. Zhang, J. Tellam, R. Sougrat, F. Laquai, D. M. DeLongchamp, J. R. Durrant, I. McCulloch, *Nat. Mater.* **2020**, *19*, 559.

[41] W. Huang, Q. He, Y. Hu, Y. Li, *Angew. Chem. Int. Ed.* **2019**, *58*, 8944.

[42] L. Dai, A. Dong, X. Meng, H. Liu, Y. Li, P. Li, B. Wang, *Angew. Chem. Int. Ed.* **2023**, *62*, e202300224.

[43] Z. Mi, T. Zhou, W. Weng, J. Unruangsri, K. Hu, W. Yang, C. Wang, K. A. I. Zhang, J. Guo, *Angew. Chem. Int. Ed.* **2021**, *60*, 9642.

[44] Y.-N. Liu, C.-C. Shen, N. Jiang, Z.-W. Zhao, X. Zhou, S.-J. Zhao, A.-W. Xu, *ACS Catal.* **2017**, *7*, 8228.

[45] L. Liu, Q. Liu, R. Li, M.-S. Wang, G.-C. Guo, *J. Am. Chem. Soc.* **2021**, *143*, 2232.

[46] G. Li, B. Zhang, J. Wang, H. Zhao, W. Ma, L. Xu, W. Zhang, K. Zhou, Y. Du, G. He, *Angew. Chem. Int. Ed.* **2019**, *58*, 8468.

[47] X. Yang, Y. Zhang, B. Zhang, S. Zhang, X. Liu, G. Li, D. Chu, Y. Zhao, G. He, *J. Mater. Chem. C* **2020**, *8*, 16326.

[48] G. Li, L. Xu, W. Zhang, K. Zhou, Y. Ding, F. Liu, X. He, G. He, *Angew. Chem. Int. Ed.* **2018**, *57*, 4897.

[49] X. Yang, B. Zhang, Y. Gao, C. Liu, G. Li, B. Rao, D. Chu, N. Yan, M. Zhang, G. He, *Adv. Sci.* **2022**, *9*, 2101652.

[50] G. Li, R. Song, W. Ma, X. Liu, Y. Li, B. Rao, G. He, *J. Mater. Chem. A* **2020**, *8*, 12278.

[51] G. Li, K. Zhou, Q. Sun, W. Ma, X. Liu, X. Zhang, L. Zhang, B. Rao, Y.-L. He, G. He, *Angew. Chem. Int. Ed.* **2022**, *61*, e202115298.

[52] S. Lin, K. Kitamoto, H. Ozawa, K. Sakai, *Dalton Trans.* **2016**, *45*, 10643.

[53] L. Li, R. G. Hadt, S. Yao, W.-Y. Lo, Z. Cai, Q. Wu, B. Pandit, L. X. Chen, L. Yu, *Chem. Mater.* **2016**, *28*, 5394.

[54] K. Kitamoto, K. Sakai, *Chem. Commun.* **2016**, *52*, 1385.

[55] J. B. Beck, S. J. Rowan, *J. Am. Chem. Soc.* **2003**, *125*, 13922.

[56] D. B. Shinde, G. Sheng, X. Li, M. Ostwal, A.-H. Emwas, K.-W. Huang, Z. Lai, *J. Am. Chem. Soc.* **2018**, *140*, 14342.

[57] W. Li, Z. Zhao, W. Hu, Q. Cheng, L. Yang, Z. Hu, Y. A. Liu, K. Wen, H. Yang, *Chem. Mater.* **2020**, *32*, 8553.

[58] S. Dey, *Small* **2019**, *15*, 1900134.

[59] X. Chen, S. Shen, L. Guo, S. S. Mao, *Chem. Rev.* **2010**, *110*, 6503.

[60] H. G. Kim, P. H. Borse, W. Choi, J. S. Lee, *Angew. Chem. Int. Ed.* **2005**, *44*, 4585.

[61] D. Xu, B. Cheng, S. Cao, J. Yu, *Appl. Catal. B: Environ.* **2015**, *164*, 380.

[62] H.-X. Zhang, Q.-L. Hong, J. Li, F. Wang, X. Huang, S. Chen, W. Tu, D. Yu, R. Xu, T. Zhou, J. Zhang, *Angew. Chem. Int. Ed.* **2019**, *58*, 11752.

[63] Y. Liu, B. Li, Z. Xiang, *Small* **2021**, *17*, 2007576.

[64] J. Greeley, T. F. Jaramillo, J. Bonde, I. Chorkendorff, J. K. Nørskov, *Nat. Mater.* **2006**, *5*, 909.

[65] H. Li, C. Tsai, A. L. Koh, L. Cai, A. W. Contryman, A. H. Fragapane, J. Zhao, H. S. Han, H. C. Manoharan, F. Abild-Pedersen, J. K. Nørskov, X. Zheng, *Nat. Mater.* **2016**, *15*, 48.